Surface morphology and magnetic interactions in $Ni_{0.5}Co_{0.5}FeCrO_4$ sintered at different temperatures.

Nehal Ahmed[a], V. B. Kawade[b], Y. A. Vijapure[c], G. H. Kale[d], R. H. Kadam[e],S.M. Kabbur[f],S.B. Shelke[a*]

[a]*Physics Department, S. M. P. College, Murum, Dist. Osmanabad (M.S.) India*

[b]*Physics Department, L. L. D. M. Mahavidyalaya, Parali (V), Dist. Beed (M.S.) India*

[c]*Chemistry Department, Shrikrishna Mahavidyalaya, Gunjoti, Dist. Osmanabad (M.S.) India*

[d]*Electronics Department, Y. C. College, Tuljapur, Dist. Osmanabad (M.S.) India*

[e]*Physics Department, Shrikrishna Mahavidyalaya, Gunjoti, Dist. Osmanabad (M.S.) India*

[f]*Physics Department Shri Shivaji Mahavdyalaya, Barshi, Dist. Solapur(M.S.)India*

Abstract

Sol-gel auto-combustion synthesized $Ni_{0.5}Co_{0.5}FeCrO_4$ ferrite nanoparticles were sintered at four different temperatures. As depicted by thermo-gravimetric analysis the major weight loss is occurred between the temperatures 500^0C to 600^0. The X-ray diffraction peaks observed are identified by the crystal planes (220), (311), (222), (400), (422), (333), (440), (533) which belongs to cubic spinel structure with space group Fd3m. The other structural parameters like lattice constant, X-ray density, porosity and crystallite size were calculated by using XRD data. The sufficiently broadening of the peaks confirms the nanometer size of the synthesized powders. With increasing the sintering temperature the broadening slightly reduces which increases the size of the crystallite. The surface morphology and average grain size was studied by using SEM images. The magnetic properties such as saturation magnetization, coercivity, remnant magnetization were studied by using room temperature VSM technique. Increasing sintering temperature increases the saturation magnetization and coercivity.

Keywords: *Crystallite size, sintering temperature, saturation magnetization.*

Introduction:

Nickel ferrite and cobalt ferrites belongs to the ferrites with spinel structure having general chemical formula MFe_2O_4, where M is the divalent metal ion like Ni^{2+}, Co^{2+}, Mn^{2+}, Mg^{2+}, Fe^{2+}, Cu^{2+}, Zn^{2+} etc. The metal ions in spinel ferrites are distributed over two interstitial sites tetrahedral – A and/or octahedral – B. Distribution of divalent metal ion towards tetrahedral – A and trivalent Fe^{3+} ions towards octahedral – B sites produces the normal spinels. The distribution of metal ions over tetrahedral and octahedral sites decides

the electric and magnetic properties of ferrites [1-2]. Those ferrites having high chemical and thermal stability are appropriate for different applications, like memory devices [3], sensors [4], microwave devices [5], Li-ion batteries [6] etc.

The addition of chromium in nickel – cobalt ferrite significantly changes the electrical and magnetic properties [7]. Nickel and cobalt ferrites are inverse ferrites and hence for $x \leq 1$, nickel ferrite shows structure of inverse spinel and for $x > 1$, the inverse structure converted into normal structure [8]. The crystal structure of ferrite, cation distribution, synthesis route, sintering conditions, amount and type of impurity addition decides the electric and magnetic properties of ferrites. Same ferrite with different crystalline size shows different properties. The electrical and magnetic properties even structural properties of ferrites at nano-crystalline phase shows significantly difference than the bulk one. Sintering temperature also affects on the crystallite size and also electrical and magnetic properties [9-12]. As per literature review no reports are available on the structural and magnetic properties of $Ni_{0.5}Co_{0.5}CrFeO_4$ composition with varying sintering temperature. In the present paper we have presented the results on structural and magnetic properties of $Ni_{0.5}Co_{0.5}CrFeO_4$ sintered at 500^0C, 600^0C, 700^0C and 800^0C for 6h.

Experimental:

Metal nitrates with high purity (99%) of Nickel nitrate ($Ni(NO_3)_2{\cdot}3H_2O$), cobalt nitrate ($Co(NO_3)_2{\cdot}3H_2O$), ferric nitrate ($Fe(NO_3)_3{\cdot}9H_2O$), chromium nitrate ($Cr(NO_3)_3{\cdot}9H_2O$), citric acid ($C_6H_8O_7{\cdot}H_2O$) were used as starting materials for the preparation of $Ni_{0.5}Co_{0.5}FeCrO_4$ ferrite nanoparticles. The synthesis method used for the preparation of sample was sol-gel auto-combustion technique. The metal nitrates are taken in their weight proportion and mixed thoroughly in minimum amount distilled water. Citric acid was added in the mixture with molar ratio of 1:3 with metal nitrates. The mixture is stirred continuously by using magnetic stirrer with hot plate. The reaction was carried out in open atmosphere at constant temperature of 90^0C. The pH of the solution was maintained at 7 by adding the liquid ammonia with continuous stirring. The continuous heating evaporates the water content from the solution and after some time the mixture is converted in to dark brown gel. After elimination of water content from the mixture, it gets burnt itself and converted into fine brown ash. The obtained ash was divided into four equal parts and annealed finally at four different temperatures 500^0C, 600^0C, 700^0C and 800^0C respectively.

The X-ray diffraction patterns of all the samples of $Ni_{0.5}Co_{0.5}FeCrO_4$ sintered at four different temperatures were recorded at room temperature using CuKα radiation on Ultima-IV Rigaku X-ray diffractometer. The average grain size and surface morphology was studied by using field effect scanning electron micrographs. The magnetic parameters such as saturation magnetization, magneton number, remnant magnetization, coercivity were studied by using VSM technique. All the hysteresis loops ware taken at room temperature and the applied field was 0.5 T.

Results and discussion:

The thermo-gravimetric obtained for $Ni_{0.5}Co_{0.5}FeCrO_4$ is shown in Fig. 1 and it is that between the temperatures 100^0C to 300^0, the weight loss is occurred, which may be due to the vaporization of hydroxyl group from the material. The major loss is occurred between the temperatures 500^0C to 600^0. The loss occurred in this range is related to decomposition of organic derivatives and citric acid during the reaction between initial materials. After 600^0C, the curve is almost straight with very little inclinations, which indicates that the reaction is takes place near 600^0C and the loss after 600^0 the minor loss is may be due to the oxidization of un-reacted metal nitrates.

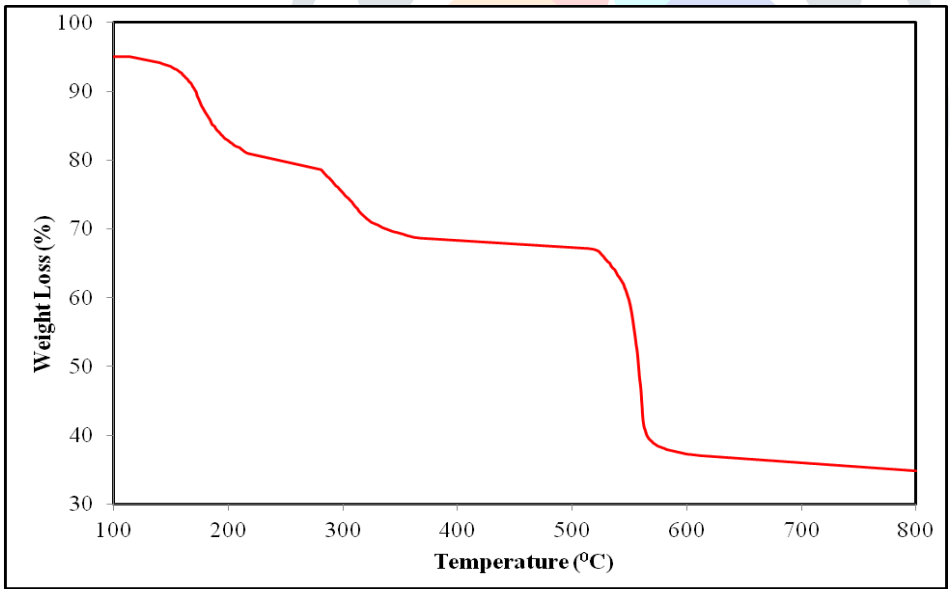

Fig. 1: Thermo-gravimetric curve of $Ni_{0.5}Co_{0.5}FeCrO_4$

Room temperature X-ray diffraction patterns of the composition $Ni_{0.5}Co_{0.5}FeCrO_4$ sintered at four temperatures (500^0C, 600^0C, 700^0C, 800^0C) are depicted in Fig. 2. Fairly matching of the diffraction peaks with standard peaks (JCPD card numbers 742081 for nickel ferrite and 791744 for cobalt ferrite) confirms the phase purity of the samples. The diffraction peaks observed are identified by the crystal planes (220),

(311), (222), (400), (422), (333), (440), (533) which belongs to cubic spinel structure with space group Fd3m. The sufficiently broadening of the peaks confirms the nanometer size of the synthesized powders. With increasing the sintering temperature the broadening slightly reduces which increases the size of the crystallite.

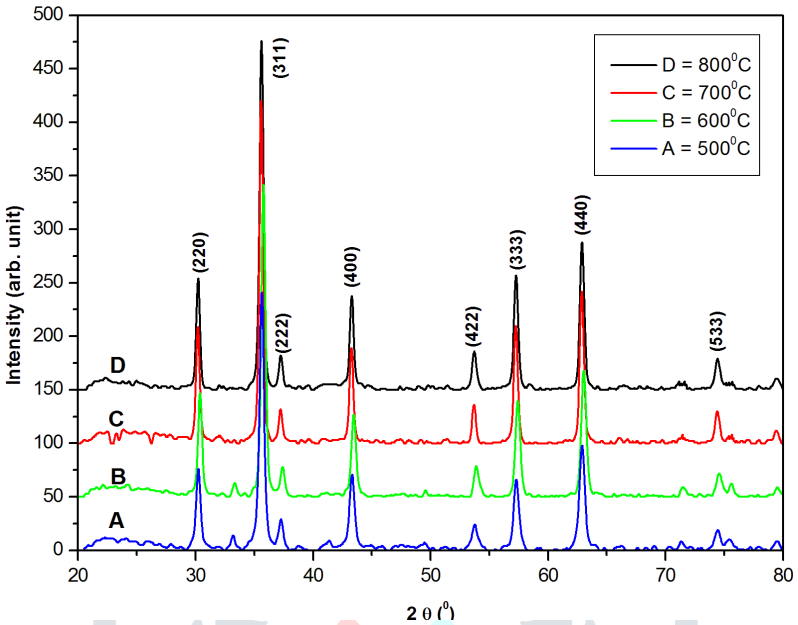

Fig. 2: X-ray diffraction patterns of $Ni_{0.5}Co_{0.5}FeCrO_4$

Lattice constant 'a' for all the samples of $Ni_{0.5}Co_{0.5}FeCrO_4$ was calculated by putting the data obtained from XRD patterns in the following relation [13],

$$a = \frac{d_{hkl}}{\sqrt{h^2 + k^2 + l^2}} \quad (1)$$

where, 'a' be the lattice constant, 'd_{hkl}' be the inter-planar distance for (hkl) plane. The values of interplaner spacing's 'd_{hkl}' obtained from XRD data are given in Table 1. Variation of lattice constant 'a' with sintering temperature is shown in Fig. 3 and the values are listed in Table 1. The lattice constant of $Ni_{0.5}Co_{0.5}FeCrO_4$ increases from 8.3245 Å to 8.3569 Å with increase in sintering temperature from 500^0C to 800^0C. The variation of lattice parameter 'a' is may be due to the oxidation states and cation distribution in tetrahedral – A and octahedral – B sites. The reduction of Fe^{3+} ions with smaller ionic radii (0.64Å) to Fe^{2+} ions with higher ionic radii (0.76Å) during the sintering process mainly increases the values of lattice parameter. Similar behaviour of lattice parameter 'a' with increasing annealing temperature is reported in literature [14].

Table 1: Lattice parameter 'a', X-ray density 'd_x', Particle size 'D_{XRD}', Bulk density 'd_B', porosity 'P' and surface area 'S' for $Ni_{0.5}Co_{0.5}FeCrO_4$.

Sintering Temperature T (°C)	a (Å)	dx (g/cm^3)	D_{XRD} (nm)	d_B (g/cm^3)	P (%)	S (m^2/g)
500	8.3245	5.3053	21.86	3.9809	33.27	68.96
600	8.3315	5.2920	23.57	4.0643	30.21	62.62
700	8.3471	5.2624	26.84	4.1232	27.63	54.21
800	8.3569	5.2437	27.73	4.2249	24.11	51.21

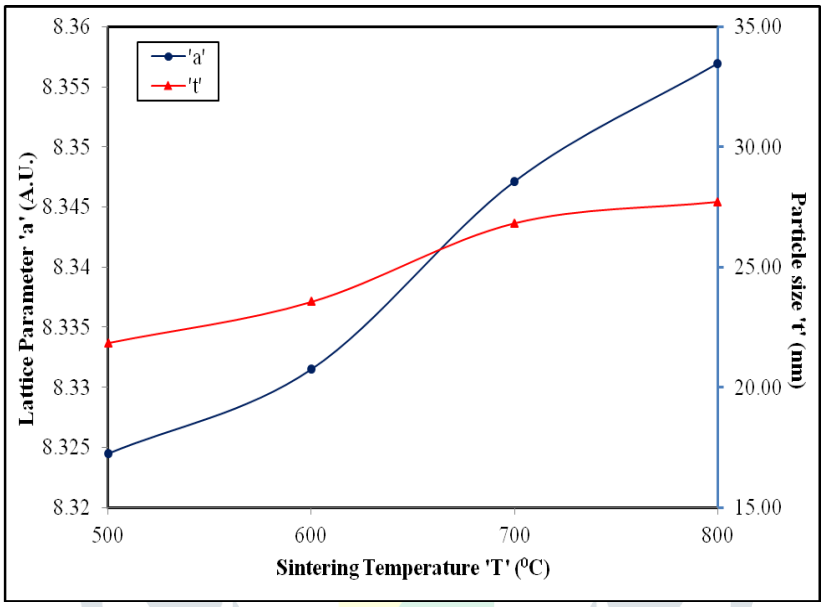

Fig. 3: Variation of Lattice parameter 'a' and particle size 't' with sintering temperature for $Ni_{0.5}Co_{0.5}FeCrO_4$.

By using the unit cell volume of cubic lattice and molecular weight in the following relation [15], X-ray density 'd_X' of all the samples was calculated;

$$d_X = \frac{nM}{NV} \qquad (2)$$

Where, n is the number of molecules per unit cell (n = 8 for cubic spinel structures), M is the molecular weight of the samples, N is Avogadro's number and V is the unit cell volume ($v = a^3$ for cubic structures). X-ray density values of all the samples calculated by using relation (2) are given in Table 1. X-ray density decreases with increase in sintering temperature. This behaviour of X-ray density is analogues with the increasing trend of lattice parameter. By converting the samples in cylindrical pellets, the bulk density 'd_B' was calculated. Following relation was used to calculate the bulk density,

$$d_B = \frac{m}{V} \quad (3)$$

Where, m is the mass of pellet and V is the volume of pellet ($V = \pi r^2 t$, where, r is the radius of pellet and t is the thickness of pellet). Bulk density 'd_B' is reduced as the sintering temperature increases.

To determine the porosity of the samples in percentage, following relation was employed,

$$P(\%) = \left(\frac{d_x - d_B}{d_x} \right) \times 100 \quad (4)$$

Calculated values of percentage porosity are listed in Table 1. It can be observed that the percentage porosity shows the decreasing trend as the sintering temperature increases. Specific surface area (S) was calculated by using the following relation,

$$S = \frac{6000}{D\rho} \quad (5)$$

Where, D is the particle diameter and ρ is the density of the particles in gm/cc. Specific surface area decreases with increase in sintering temperature, this is may be due to the increasing trend of both particle diameter and density of the samples which are inversely proportional to specific surface area.

Fig. 4 displays the Field Effect Scanning Electron Micrographs (FESEM) of the end samples sintered at lower and higher temperatures. Well defined grains are observed on the surface of the samples. The heat treatment affected on the surface structure of the samples and also on average grain size. The average grain size is varied widely in the range of 65nm to 92nm with no linear correlation with sintering temperature.

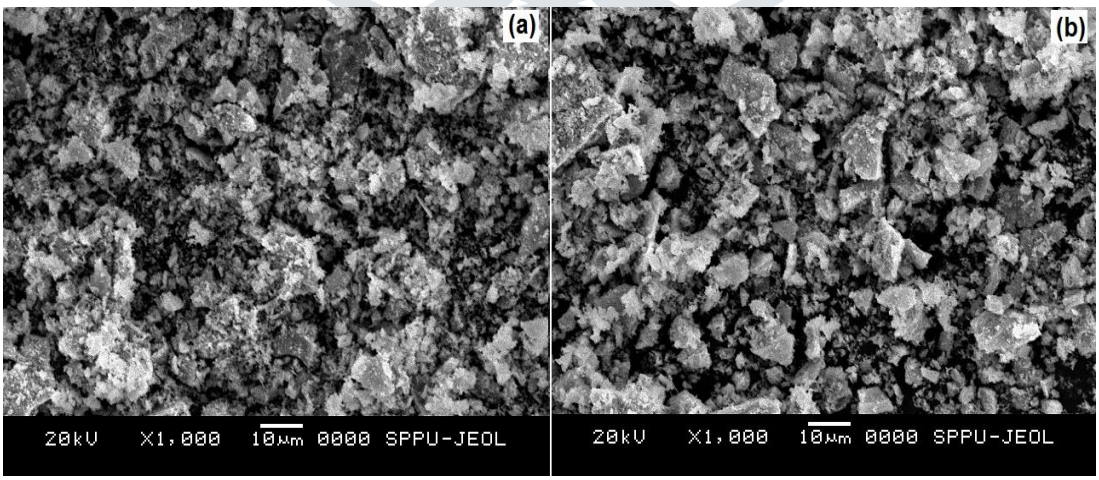

Fig. 4: Scanning electron micrographs of $Ni_{0.5}Co_{0.5}FeCrO_4$ a) 500^0C, b) 800^0C

The magnetic parameters viz. saturation magnetization (M_S), coercivity (H_C) and remnant magnetization (M_r), magneton number per formula unit (n_B) are obtained from the hysteresis loops obtained from room temperature VSM technique.

Table 2: Saturation magnetization, remnant magnetization, remnant ratio, coercivity and magnetic moment for $Ni_{0.5}Co_{0.5}FeCrO_4$

Sintering Temperature T (°C)	Saturation magnetization 'M_S' (emu/gm)	Remnant Magnetization 'M_R' (emu/gm)	Remnant ration 'R'	Coercivity 'H_C' (Oe)	Magnetic moment 'n_B' (μ_B)
500	2.1387	1.1427	1.8716	228.4	0.088
600	9.3199	5.2789	1.7655	427.5	0.384
700	26.095	15.267	1.7092	619.8	1.076
800	36.693	23.658	1.6778	827.3	1.637

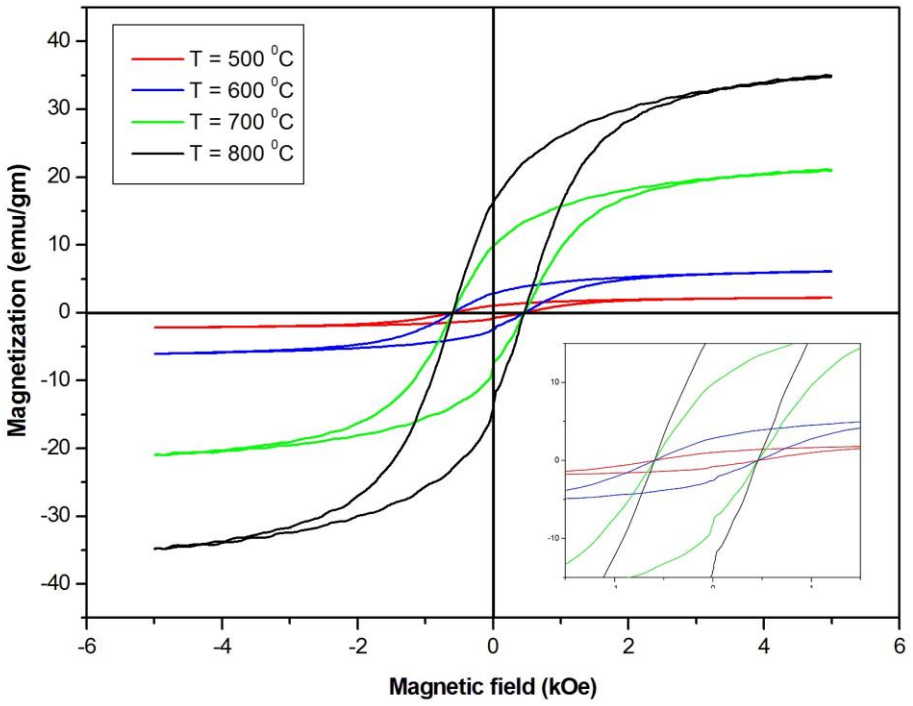

Fig. 5: Hysteresis curves of $Ni_{0.5}Co_{0.5}FeAlO_4$ (Inset shows the expanded center of hysteresis curves)

Fig. 5 shows the hysteresis curves of all the samples heated at four different temperatures. It is observed from Fig. 5 that as annealing temperature increases, saturation magnetization of the sample increases. The coercivity (H_C) values increase with increase in sintering temperature. To observe the displacement in coercivity, the expanded view of hysteresis curves is shown in the inset of Fig. 5. Inverse proportionality of coercivity with saturation magnetization is related by using the Brown's relation [16-17],

$$H_C = \frac{2K_1}{\mu_0 M_S} \quad (6)$$

The coercivity values obtained from hysteresis curves are in good agreement with the above relation. The observed magnetic moment per formula unit is calculated by using the following relation [18];

$$n_B(\text{Obs.}) = \frac{MW \times M_S}{5585} \quad (7)$$

where, n_B (Obs.) is the magnetic moment per formula unit of the samples expressed in Bohr magneton (μ_B), MW is the molecular weight of the sample under consideration and M_S is the saturation magnetization of the sample.

Conclusions:

The samples were successfully synthesized by using low temperature sol-gel auto-combustion technique. The thermo-gravimetric curve indicates that the pure ferrite phase was obtained near 600^0C. From XRD analysis, structure of the composition was confirmed as cubic spinel with space group Fd3m. The sufficiently broadening of the peaks confirms the nanometer size of the synthesized powders. As annealing temperature increases, saturation magnetization of the sample increases. The coercivity (H_C) values increase with increase in sintering temperature.

References:

[1] A. M. Dumitrescu, P. M. Samoila, V. Nica, F. Doroftei, A. R. Iordan, M. N. Palamaru, Study of the chelating / fuel agents influence on $NiFe_2O_4$ samples with potential catalytic properties; Powder Tech. 243 (2013) 9-17.

[2] M. Younas, M. Nadeem, M. Arif, R. Grossinger, Metal-semiconductor transition in $NiFe_2O_4$ nanoparticles due to reverse cationic distribution by impedance; J. App. Phys. 109 (2011) 093704-1-093704-8.

[3] M. A. Gabal, W. A. Bayoumy; Effect of composition on structural and magnetic properties of nanocrystalline $Ni_{0.8-x}Zn_{0.2}Mg_xFe_2O_4$ ferrite; Polyhedraon 29 (2010) 2569-2573.

[4] C. Xiangfeng, J. Dongli, Z. Chenmou; The preparation and gas – sensing properties of $NiFe_2O_4$ nanocubes and nanorods; Sensors and Actuators B: Chemical 123 (2007) 793-797.

[5] G. A. El-Shobaky; A. M. Turky, N. Y. Mostafa, S. K. Mohamed; Effect of preparation conditions on physicochemical, surface and catalytic properties of cobalt ferrite prepared by coprecepitation; J. Alloys. Comp. 493 (2010) 415-422.

[6] H. Zhao, H. Jia, S. Wang, D. Xue, Z. Zheng; Fabrication and application of MFe_2O_4 (M = Zn, Cu) nanoparticles as anodes for Li ion batteries; J. Exper. Nanosci. 6 (2011) 75-83.

[7] S. H. Lee, S. J. Yoon, G. J. Lee, H. S. Kim, C. H. Yo, K. Ahn, D. H. Lee, K. H. Kim; Electrical and magnetic properties of $NiCr_xFe_{2-x}O_4$ spinel; Mater. Chem. Phys. 61 (1999) 147-152.

[8] P. F. Bongers, Philips. Tech. Rev. 28 (1967) 13.

[9] G. Mustafa, M. U. Islam, W. Zhang, Y. Jamil, M. A. Iqbal, M. Hussain, M. Ahmad; Temperature dependent structural and magnetic properties of cerium substituted Co-Cr ferrite prepared by auto-combustion method; J. Magn. Magn. Mater. 378 (2015) 409-416.

[10] M. Mozaffari, J. Amighian; Preparation of Al-substituted Ni ferrite powders via mechanochemcial processing; J. Magn. Magn. Mater; 260 (2003) 244-249.

[11] M. A. Amer, T. M.Meaz, A. G. Mostafa, H. F. El-Ghazallly; Annealing effect on the structural and magnetic properties of the $CuAl_{0.6}Cr_{0.2}Fe_{1.2}O_4$ nano-ferrites; Mare. Res. Bull. 67 (2015) 207-214.

[12] A. Verma, T. C. Goel, R. G. Mendiratta, P. Kishan; Magnetic properties of nickel-zinc ferrites prepared by the citrate precursor method; J. Magn. Magn. Mater. 208 (2000) 13-19.

[13] Rabia Pandit, K.K. Sharma , Pawanpreet Kaur, R.K. Kotnala, Jyoti Shah, Ravi Kumar. Effect of Al^{3+} substitution on structural, cation distribution, electrical and magnetic properties of $CoFe_2O_4$, J. Phys. Chem. Solids 75(2014) 558–569.

[14] F. L. Zabotto, A. J. Guddi, J. A. Eiras, A. J. Aparecido de Oliveira, D. Garcia; Influence of the sintering temperature on the magnetic and electric properties of $NiFe_2O_4$ ferrites; Materials research 15 (2012) 428-433.

[15] M. George, S. S. Nair, A. M. John, P. A. Joy, M. R. Anantharaman, Structural, magnetic and electrical properties of the sol-gel prepared $Li_{0.5}Fe_{2.5}O_4$ fine particles; J. Phys. D: Appl. Phys. 39 (2006) 900-910.

[16] Vivek Choudhari, R. H. Kadam, M. L. Mane, S. E. Shirsath, A. B. Kadam, D. R. Mane; Effect of La^{3+} impurity on magnetic and electrical properties of Co-Cu-Cr-Fe nanoparticles; J. Nanosci. Nanotech. 14 (2014) 1-8.

[17] J. M. D. Coey, Rare earth, permanent magnetism; John Wiley and Sons, New York (1996).

[18] R. H. Kadam, S. T. Alone, A. S. Gaikwad, A. P. Birajdar, S. E. Shirsath; Al^{3+} ions dependent structural and magnetic properties of Co-Ni nano-alloys; J. Nanosci. Nanotech. 13 (2013) 1-7.